4. V. Rajeshkumar and S. Raghavan, A compact asymmetric monopole antenna with electrically coupled SRR for WiMAX/WLAN/UWB applications, Microwave Opt Technol Lett 57 (2015), 2194–2197.
5. G. H. Li, H. Q. Zhai, L. Li, and C. H. Liang, A nesting-L slot antenna with enhanced circularly polarized bandwidth and radiation, IEEE Antennas Wireless Propag Lett 13 (2014), 225–228.
6. R. Zaker and A. Abdipour, Dual-wideband circularly-polarized slot antenna using folded L-shaped stub, Electron Lett 47 (2011), 361–363.
7. C. J. Wang, M. H. Shih, and L. T. Chen, A wideband open-slot antenna with dual-band circular polarization, IEEE Antennas Wireless Propag Lett 14 (2015), 1306–1309.
8. CST Studio Suite, Computer simulation technology, CST Corporation, Darmstadt, Germany, 2010.

VERY-LOW-PROFILE HYBRID OPEN-SLOT/CLOSED-SLOT/INVERTED-F ANTENNA FOR THE LTE SMARTPHONE

Kin-Lu Wong and Wan-Chin Wu
Department of Electrical Engineering, National Sun Yat-sen University, Kaohsiung, 80424, Taiwan; Corresponding author: wongkl@ema.ee.nsysu.edu.tw

Received 2 November 2015

ABSTRACT: *A very-low-profile hybrid antenna for the LTE smartphone was presented. The antenna structure was mainly formed by a T-shaped open slot disposed on the main circuit board inside the smartphone casing and a metallic patch printed on the inner surface of the frame around the smartphone casing. The antenna with the T-shape open slot and the on-frame metallic patch had a very low profile of 3 mm. By using two feeds (low-band and high-band feeds) across the two arms of the T-shape open slot and connected to the on-frame metallic patch, hybrid resonant modes including the open-slot antenna (OSA) mode, the closed-slot antenna (CSA) mode, and the inverted-F antenna (IFA) mode could be generated to form two operating bands for the LTE operation. The low band could cover the 824–960 MHz band for the LTE band 5 and 8 operation. The high band can cover the 1710–2690 MHz band for the LTE band 10, 15, and 16 operation. The techniques on exciting the hybrid resonant modes with good impedance matching for the proposed very-low-profile antenna were addressed in this study. Experimental data of the fabricated antenna were also presented to verify the simulation results.* © 2016 Wiley Periodicals, Inc.
Microwave Opt Technol Lett 58:1572–1577, 2016; View this article online at wileyonlinelibrary.com. DOI 10.1002/mop.29863

Key words: *mobile antennas; smartphone antennas; inverted-F antennas; slot antennas; open-slot antennas; hybrid antennas; very-low-profile antennas; LTE antennas*

1. INTRODUCTION

The internal antennas with a low profile or narrow ground clearance have been very attractive for the modern smartphone application. Such low-profile antennas can allow the large display panel to be employed in the modern smartphone. However, very few internal long-term evolution (LTE) or wireless wide area network (WWAN) antennas for the smartphone have been reported to have a very low profile of 3 mm [1,2]. To achieve the very low profile, the reported antennas in Ref. [1,2] are constructed based on the loop antenna structure [3–5] and the loop resonant modes are generated to cover the desired operating bands. It is also noted that the antenna structure in Ref. [1] requires having a wider ground clearance of width 5 mm at two ends thereof, so as to achieve better antenna performance. The antenna structure in Ref. [2] requires a three-dimensional loop metal pattern, which complicates the antenna design and fabrication. In order to provide more promising very-low-profile antennas for the modern smartphone application, the present study is motivated.

In this study, different from only the loop resonant modes applied in Ref. [1,2], a very-low-profile antenna with hybrid resonant modes generated is presented for the modern smartphone application. The hybrid resonant modes include the open-slot antenna (OSA) mode [6–9], the closed-slot antenna (CSA) mode [10,11], and the inverted-F antenna (IFA) mode [12–14]. These hybrid resonant modes are generated to form two operating bands for the LTE operation. The low band can cover the 824–960 MHz band for the LTE band 5 and 8 operation, and the high band can cover the 1710–2690 MHz band for the LTE band 10, 15, and 16 operation [15].

To generate the hybrid resonant modes, the antenna is mainly formed by a T-shape open slot disposed on the main circuit board inside the smartphone casing and a metallic patch printed on the inner surface of the frame around the smartphone casing. The slot opening of the T-shape open slot is disposed at the on-frame metallic patch. The total profile of the T-shape open slot is 3 mm only. Two feeds (low-band and high-band feeds) passing through the two arms of the T-shape open slot and connected to the on-frame metallic patch are applied. The low-band feed is loaded with a series inductor and a band-pass matching circuit, whereas the high-band feed has a loaded series capacitor and a low-pass matching circuit.

With the proposed feed arrangement, the low-band feed excites a section of the on-frame metallic patch as a radiator and leads to the IFA mode generated. On the other hand, the high-band feed excites the T-shape open slot or part of the T-shape open slot as a radiator and leads to the OSA mode and CSA mode generated. The matching circuits in the low-band and high-band feeds cause an additional resonance in the desired low and high bands, thereby greatly increasing the antenna bandwidth. The antenna structure is described in detail in this study. Based on the feed arrangement, the techniques on generating the hybrid resonant modes are addressed. The antenna is also fabricated and tested to verify the simulation results.

2. ANTENNA STRUCTURE AND OPERATING PRINCIPLE

2.1. Antenna Structure and Feed Arrangement

Figure 1 shows the geometry of the very-low-profile hybrid antenna for the LTE smartphone. The side-view and front-view photos of the fabricated antenna are also shown in Figure 2 for better understanding of the antenna structure. The antenna consists of a T-shape open slot disposed on the main circuit board and an on-frame metallic patch orthogonal to the main circuit board. The LTE smartphone is considered to have a 6-inch large display panel (not shown in the figure), and the main circuit board therein is of dimensions 80×150 mm^2. A 0.8-mm thick FR4 substrate of relative permittivity 4.4 and loss tangent 0.02 is used as the main circuit board in the study. The T-shape open slot disposed in the device ground plane printed on the main circuit board has a uniform slot width of 2 mm and is spaced 1 mm to the short edge (top or bottom edge) of the main circuit board. The total profile of the T-shape open slot is hence only 3 mm to the short edge of the main circuit board, which is much lower than that (7 mm) of a reported T-shape open-slot antenna for the LTE tablet computer application [16].

A 0.8-mm thick FR4 substrate is also used as the frame around the smartphone (only the frame portion along the short edge is shown in the figure), and the width of the frame is selected to be 6 mm for a slim smartphone. The on-frame metallic patch is printed on the inner surface of the frame. The metallic patch has a simple rectangular shape of size 6 × 80 mm^2 and is separated into two sections. The longer section has a length of 60 mm and can be treated to be short-circuited to the ground plane at its one end. The longer section is excited at port 1 through a low-band feed placed close to the shorting end thereof. In this case, an IFA structure is formed (see the purple dashed region indicated in the figure). The resonant mode of the IFA is excited by the low-band feed to occur at about 830 MHz in the antenna's low band. Note that the low-band feed consists of a series inductor L_a (5.1 nH), a band-pass matching circuit with L_1 (5.6 nH) and C_1 (3.0 pF), and a fine-tuning capacitor C_f (2.4 pF). The low-band feed leads to a widened bandwidth for the antenna's low band to cover the 824–960 MHz band for the LTE band 5 and 8 operation. Detailed effects of the low-band band will be discussed in Section 2.2 with the aid of Figures 4 and 5.

On the other hand, the shorter section of the on-frame metallic patch has a length of 18.5 mm. The shorter section is connected to the high-band feed and excited at port 2. The high-band feed has a series capacitor C_a (0.8 pF) and a low-pass matching circuit with C_2 (0.1 pF) and L_2 (2.2 nH). With the antenna structure and high-band feed, an OSA structure and a CSA structure are formed. The shorter section mainly serves as an extended ground wall of the OSA (see the red slot path indicated in the figure), whereas both the shorter and longer sections

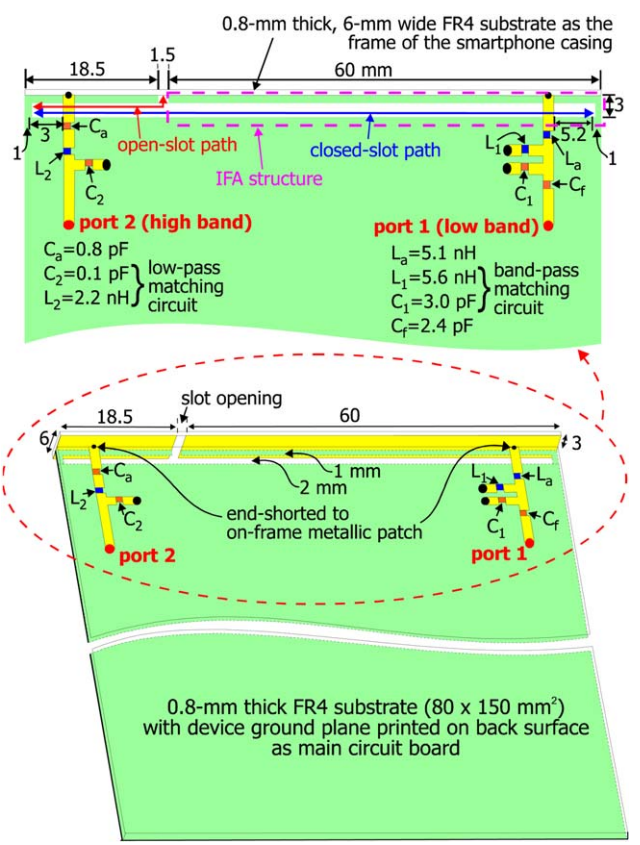

Figure 1 Geometry of the very-low-profile hybrid antenna for the LTE smartphone. [Color figure can be viewed in the online issue, which is available at wileyonlinelibrary.com]

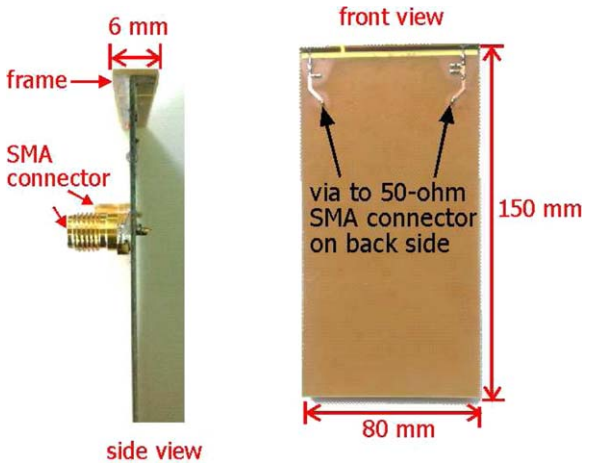

Figure 2 Photos of the fabricated antenna. [Color figure can be viewed in the online issue, which is available at wileyonlinelibrary.com]

of the on-frame metallic patch serve as an extended ground wall of the CSA (see the blue slot path indicated in the figure). A resonant mode (0.25-wavelength slot mode) of the OSA is excited at about 1.8 GHz, and a resonant mode (1.0-wavelength slot mode) of the CSA is excited at about 3.0 GHz. The high-band feed also leads to an additional resonance at about 2.4 GHz, which combines the OSA mode and the CAS mode to form the high band of 1710–2690 MHz for the LTE band 10,

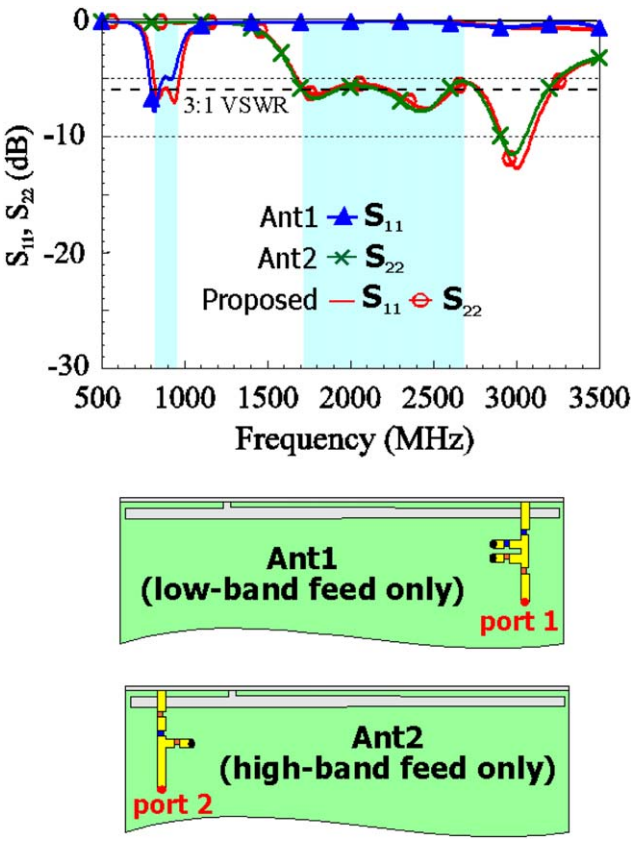

Figure 3 Simulated S parameters for the proposed antenna, the case with the low-band feed only (Ant1), and the case with the high-band feed only (Ant2). [Color figure can be viewed in the online issue, which is available at wileyonlinelibrary.com]

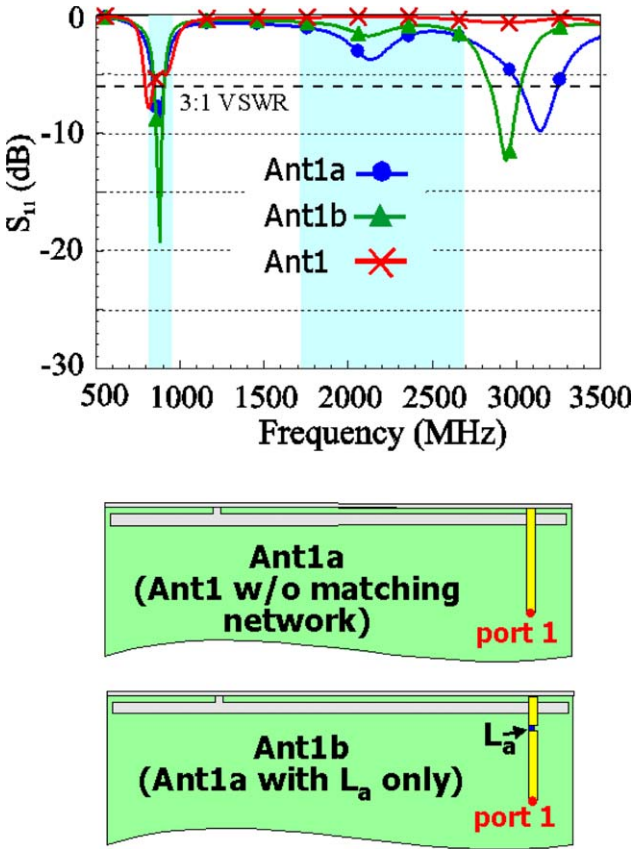

Figure 4 Simulated S_{11} for Ant1, Ant1 without L_a, L_1, C_1, and C_f (Ant1a), and Ant1a with L_a (Ant1b). [Color figure can be viewed in the online issue, which is available at wileyonlinelibrary.com]

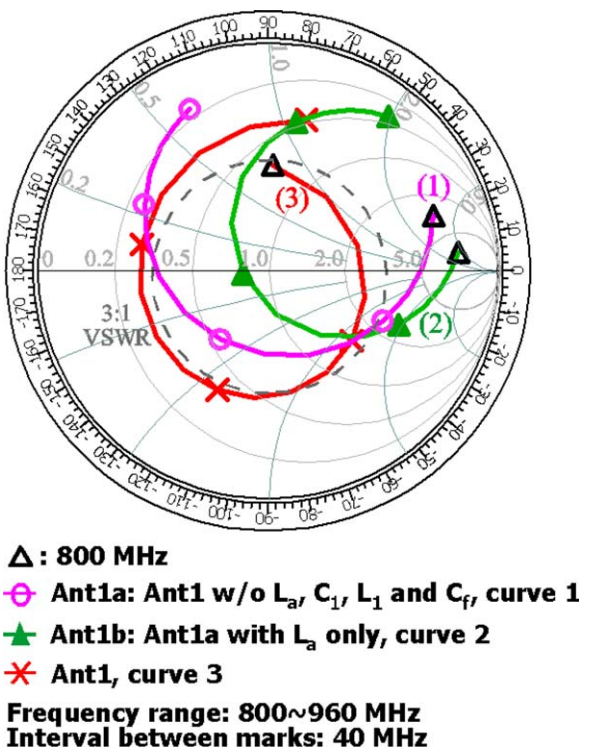

Figure 5 Simulated input impedance on the Smith chart for Ant1a (curve 1), Ant1b (curve 2), and Ant1 (curve 3). [Color figure can be viewed in the online issue, which is available at wileyonlinelibrary.com]

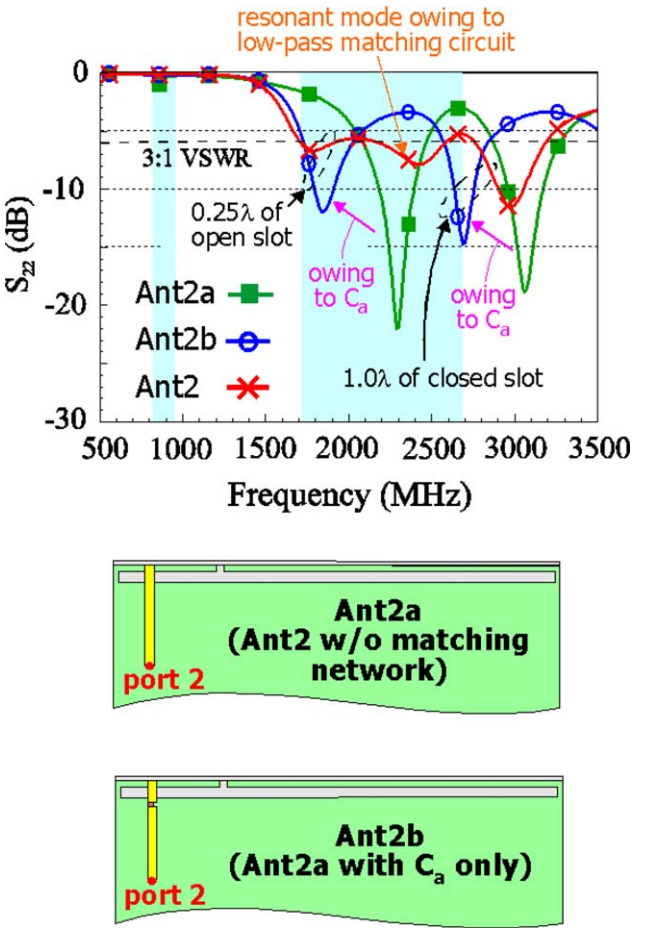

Figure 6 Simulated S_{22} for Ant2, Ant2 without C_a, L_2, and C_2 (Ant2a), and Ant2a with C_a (Ant2b). [Color figure can be viewed in the online issue, which is available at wileyonlinelibrary.com]

15, and 16 operation. Detailed effects of the high-band band will be discussed in Section 2.2 with the aid of Figures 6 and 7.

2.2. Operating Principle on Generating Hybrid Resonant Modes

The generation of the hybrid modes consisting of the IFA mode, the OSA mode, and the CSA mode is addressed in this section. To begin with, the effects of the low-band and high-band feeds are discussed. Figure 3 shows the simulated S parameters for the proposed antenna, the case with the low-band feed only (Ant1), and the case with the high-band feed only (Ant2). The simulated results are obtained using the high-frequency structure simulator HFSS simulation software version 15 [17]. Results show that the S_{11} for Ant1 covers the 824–960 MHz band (the antenna's low band, see the shaded region at lower frequencies in the figure). On the other hand, the S_{22} for Ant2 covers the 1710–2690 MHz band (the antenna's high band, see the shaded region at higher frequencies in the figure). The antenna's low and high bands can be, respectively, controlled by the low-band and high-band feeds.

To analyze the low-band matching network effects, Figure 4 shows the simulated S_{11} for Ant1, Ant1 without L_a, L_1, C_1, and C_f (Ant1a), and Ant1a with L_a (Ant1b). The corresponding input impedance curves for Ant1, Ant1a, and Ant1b are also shown in Figure 5. For Ant1a, an IFA resonant mode occurred at about 830 MHz is seen (see Fig. 4). However, the impedance bandwidth is narrow and cannot cover the desired 824–960 MHz band. To achieve a wider bandwidth, the impedance matching

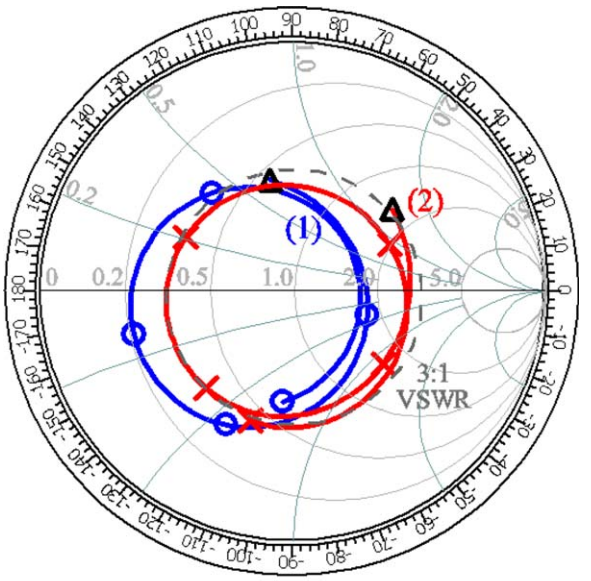

Figure 7 Simulated input impedance on the Smith chart for Ant2b (curve 1) and Ant2 (curve 2). [Color figure can be viewed in the online issue, which is available at wileyonlinelibrary.com]

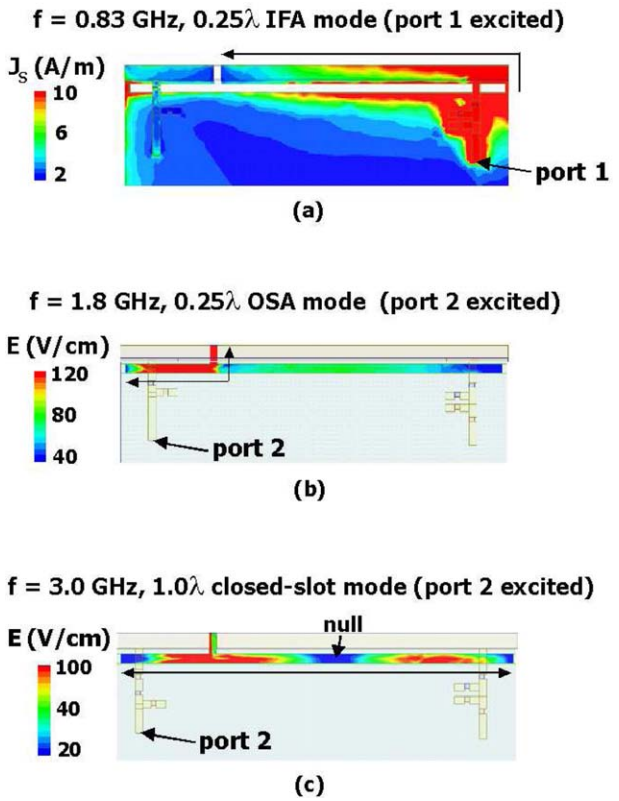

Figure 8 (a) Simulated surface current distribution at 0.83 GHz, (**b**) simulated electric field distribution at 1.8 GHz, and (**c**) simulated electric field distribution at 3.0 GHz for the proposed antenna. [Color figure can be viewed in the online issue, which is available at wileyonlinelibrary.com]

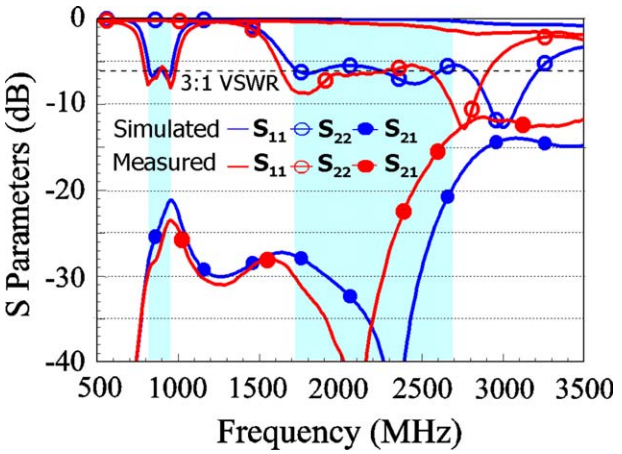

Figure 9 Measured and simulated S parameters for the fabricated antenna. [Color figure can be viewed in the online issue, which is available at wileyonlinelibrary.com]

of the IFA mode needs to be improved. For this purpose, the inductor L_a (5.1 nH) is first added (see Ant1b). From the comparison of curve 1 for Ant1a and curve 2 for Ant1b shown in Figure 5, it is seen that curve 2 passes through about the center of the Smith chart. That is, better impedance matching of the IFA mode is obtained by adding the inductor L_a. This is because the IFA structure has a very low profile (3 mm here) which generally shows a large capacitive component in the antenna's input impedance. Hence, the adding of the series inductor L_a can effectively compensate for it to achieve improved impedance matching.

Then, by further adding the band-pass matching circuit (L_1 and C_1) and the fine-tuning capacitor C_f (that is, Ant1 is formed), an additional resonance in the vicinity of the IFA mode can be generated to widen the low-band bandwidth [18,19]. Dual-resonance behavior is hence seen in the antenna's low band (see Fig. 4) and curve 3 for Ant1 is also seen to be close to a loop-like curve (see Fig. 5). In addition, the spurious modes at higher frequencies can be suppressed to increase the isolation between port 1 and port 2.

The high-band matching network effects are also analyzed. Figure 6 shows the simulated S_{22} for Ant2, Ant2 without C_a, L_2, and C_2 (Ant2a), and Ant2a with C_a (Ant2b). There are three resonant modes generated by Ant2. The lower mode at about

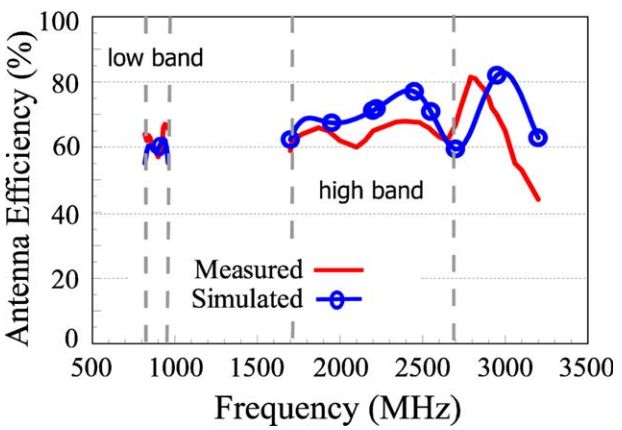

Figure 10 Measured and simulated antenna efficiencies for the fabricated antenna. [Color figure can be viewed in the online issue, which is available at wileyonlinelibrary.com]

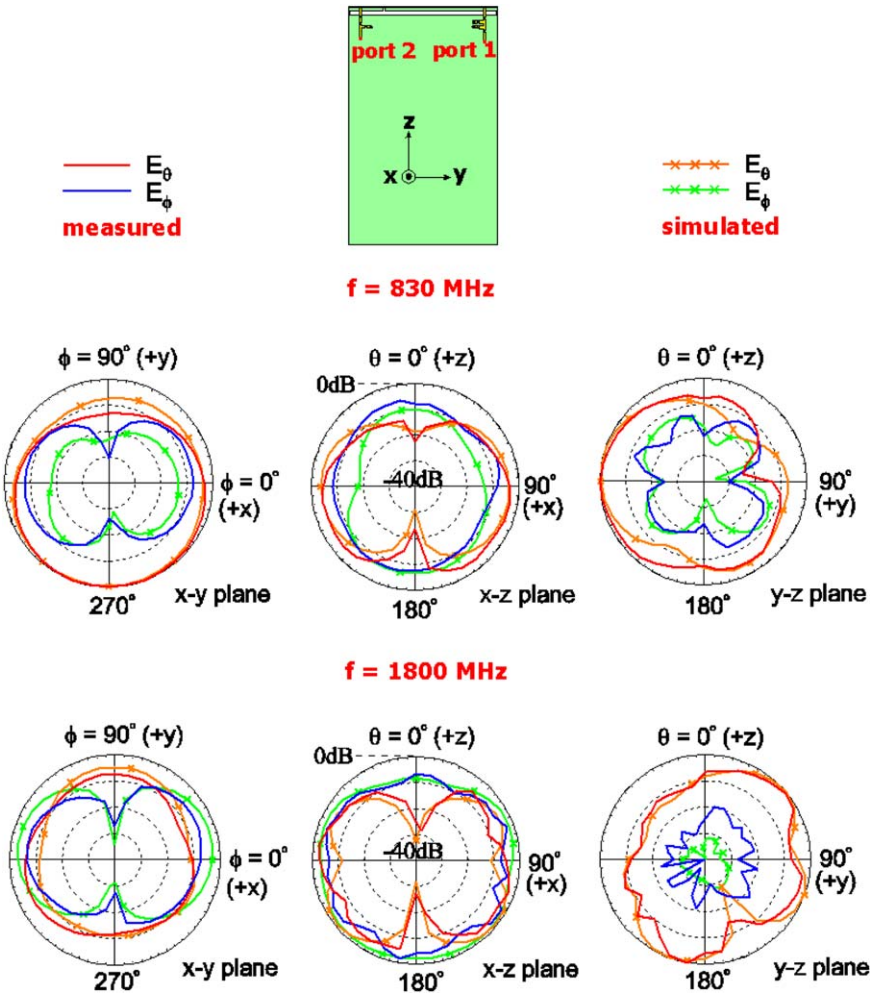

Figure 11 Measured and simulated radiation patterns for the fabricated antenna. [Color figure can be viewed in the online issue, which is available at wileyonlinelibrary.com]

1.8 GHz and the higher mode at about 3.0 GHz are, respectively, the 0.25-wavelength open-slot mode and the 1.0-wavelength closed-slot mode, whereas the middle mode is owing to the low-pass matching circuit (C_2 and L_2, see the curve for Ant2b vs. the curve for Ant2) [20,21]. Note that it is owing to the series capacitor C_a that the lower and higher modes are, respectively, shifted to lower frequencies (see the curve for Ant2a vs. the curve for Ant2b).

Effects of the low-pass matching circuit (C_2 and L_2) can be seen more clearly in Figure 7, in which the simulated input impedance on the Smith chart for Ant2b and Ant2 is presented. It is seen that the low-pass matching circuit shifts the impedance curve of Ant2b (curve 1) into 3:1 VSWR circle (see curve 2). A much wider high band to cover the 1710–2690 MHz band is hence obtained.

To further clearly identify the resonant modes excited at 0.83, 1.8, and 3.0 GHz for the proposed antenna, the simulated surface current distribution at 0.83 GHz is shown in Figure 8(a) and the simulated electric field distributions at 1.8 and 3.0 GHz in the T-shape open slot are shown in Figures 8(b) and 8(c). When port 1 is excited, strong electric fields on the longer section of the on-frame metallic patch are seen [see Fig. 8(a)]. The results indicate that the IFA mode is generated at 0.83 GHz. When port 2 is excited, strong electric fields in the open-slot path at 1.8 GHz and in the closed-slot path at 3.0 GHz are seen. There are no nulls in the open-slot path [see Fig. 8(b)], indicating that a 0.25-wavelength OSA mode is generated. On the other hand, the electric-field distribution shown in Figure 3(c) indicates that a 1.0-wavelength CSA mode is generated. That is, the hybrid modes of the IFA mode, the OSA mode, and the CSA mode are generated in the proposed antenna.

3. EXPERIMENTAL RESULTS

Experimental results are obtained by testing the fabricated antenna shown in Figure 2. The measured and simulated S parameters for the fabricated antenna are shown in Figure 9. The measured S_{11}, S_{22}, and S_{21} curves are seen to agree with the simulated results. The measured isolation in the low band is better than 23 dB ($S_{21} < -23$ dB). For the high band, the measured isolation is better than 13 dB ($S_{21} < -13$ dB). The measured and simulated antenna efficiencies for the fabricated antenna are also presented in Figure 10. The radiation characteristics are measured in a far-field anechoic chamber. The measured antenna efficiency includes the mismatching losses, and fair agreement between the measurement and simulation is also seen. The measured antenna efficiency is about 57%–66% in the low band and about 59%–67% in the high band. The antenna efficiency is acceptable for practical smartphone application.

Figure 11 shows the measured and simulated radiation patterns for the fabricated antenna. Typical radiation patterns at 830 and 1800 MHz are shown. The radiation patterns in three principal

planes including the x–y plane (the azimuthal plane), the x–z plane (the elevation plane orthogonal to the main circuit board), and the y–z plane (the elevation plane parallel to the main circuit board) are shown. The measured and simulated results for the E_θ and E_ϕ radiation are presented, and agreement between the measurement and simulation is also obtained.

At 830 MHz, strong radiation in the $-y$ direction or the left-hand-side direction is seen (see the patterns in the x–y and y–z plane), although port 1 for the low-band excitation is close to the right-hand side of the main circuit board. This is mainly owing to the excited surface currents on the device ground plane of the main circuit board, which also contributes to the antenna radiation. At 1800 MHz, similar behavior is observed. Strong radiation in the $+y$ direction or the right-hand side direction is seen (see the patterns in the x–y and y–z plane at 1800 MHz). Again, this is owing to the surface currents on the device ground plane excited by port 2. In general, the obtained radiation characteristics show no special distinction to those of the reported LTE antennas and are acceptable for practical smartphone applications.

4. CONCLUSION

A very-low-profile hybrid antenna with the IFA mode, OSA mode, and CSA mode excited for the LTE operation in the modern smartphone has been proposed. The antenna has also been fabricated and tested. The measured data fairly agree with the simulated results. Acceptable radiation characteristics have been obtained. With a very-low-profile of 3 mm only, the antenna can cover the 824–960 and 1710–2690 MHz bands for the LTE operation (low band covering the LTE band 5 and 8 and high band covering the LTE band 10, 15, and 16). The techniques of generating the hybrid resonant modes with good impedance matching have also been addressed. The proposed antenna is especially suitable for the modern smartphone application to accommodate a large display panel.

REFERENCES

1. K. Ishimiya, C.Y. Chiu, and J. Takada, Multiband loop handset antenna with less ground plane, IEEE Antenna Wireless Propag Lett 12 (2013), 1444–1447.
2. Y.W. Chi and K.L. Wong, Very-small-size folded loop antenna with a band-stop matching circuit for WWAN operation in the mobile phone, Microwave Opt Technol Lett 51 (2009), 808–814.
3. Y.L. Ban, Y.F. Qiang, Z. Chen, K. Kang, and J.H. Guo, A dual-loop antenna design for hepta-band WWAN/LTE metal-rimmed smartphone applications, IEEE Trans Antenna Propag 63 (2015), 48–58.
4. Y. Li, Z. Zhang, J. Zheng, and Z. Feng, Compact heptaband reconfigurable loop antenna for mobile handset, IEEE Antenna Wireless Propag 10 (2011), 1162–1165.
5. B.K. Yu, B. Jung, H.J. Lee, F.J. Harackiewicz, and B. Lee, A folded and bent internal loop antenna for GSM/DCS/PCS operation of mobile handset applications, Microwave Opt Technol Lett 48 (2006), 463–467.
6. H. Wang, M. Zheng, and S.Q. Zhang, Monopole slot antenna, US Patent No. 6618020, 2003.
7. C.I. Lin and K.L. Wong, Printed monopole slot antenna for internal multiband mobile phone antenna, IEEE Trans Antenna Propag 55 (2007), 3690–3697.
8. W.S. Chen and K.Y. Ku, Bandwidth enhancement of open slot antenna for UWB applications, Microwave Opt Technol Lett 50 (2008), 438–439.
9. K.L. Wong and P.R. Wu, Dual-wideband linear open slot antenna with two open ends for the LTE/WWAN smartphone, Microwave Opt Technol Lett 57 (2015), 1269–1274.
10. S.H. Lee, Y. Lim, Y.J. Yoon, C.B. Hong, and H.I. Kim, Multiband folded slot antenna with reduced hand effect for handsets, IEEE Antenna Wireless Propag Lett 9 (2010), 674–677.
11. K.L. Wong, Y.W. Chi, and S.Y. Tu, Internal multiband printed folded slot antenna for mobile phone application, Microwave Opt Technol Lett 49 (2007), 1833–1837.
12. S. Jeon and H. Kim, Mobile terminal antenna using a planar inverted-E feed structure for enhanced impedance bandwidth, Microwave Opt Technol Lett 54 (2012), 2133–2139.
13. K.L. Wong and C.Y. Tsai, Small-size stacked inverted-F antenna with two hybrid shorting strips for the LTE/WWAN tablet device, IEEE Trans Antenna Propag 62 (2014), 3962–3969.
14. P. Bevelacqua, Dynamically adjustable antenna supporting multiple antenna modes, US Patent No. 9892002 B2, 2015.
15. I. Poole, LTE frequency bands and spectrum allocations, available at http://www.radio-electronics.com/
16. K.L. Wong and C.Y. Tsai, Low-profile dual-wideband inverted-T open slot antenna for the LTE/WWAN tablet computer with a metallic frame, IEEE Trans Antenna Propag 63 (2015), 2879–2886.
17. ansys HFSS. [Online], Available at http://www.ansys.com/staticassets/ANSYS/staticassets/resourcelibrary/brochure/ansys-hfss-brochure-16.0.pdf, 2015.
18. K.L. Wong and L.Y. Chen, mall-size LTE/WWAN tablet device antenna with two hybrid feeds, IEEE Trans Antenna Propag 62 (2014), 2926–2934.
19. K.L. Wong and Z.G. Liao, Small-size dual-wideband monopole antenna with inductive and capacitive feeding branches for long term evolution tablet computer application, Microwave Opt Technol Lett 57 (2015), 853–860.
20. K.L. Wong and Y.J. Li, Low-profile open-slot antenna with three branch slots for triple-wideband LTE operation in the metal-framed smartphone, Microwave Opt Technol Lett 57 (2015), 2231–2238.
21. K.L. Wong and Z.G. Liao, Passive reconfigurable triple-wideband antenna for LTE tablet computer, IEEE Trans Antenna Propag 63 (2015), 901–908.

SQUARE LOOP SLOTS LOADED SUBSTRATE INTEGRATED WAVEGUIDE BASED HORN ANTENNA

Amit Patel, Alpesh Vala, Riddhi Goswami, and Keyur Mahant
Charusat Space Research Technology Centre, CHARUSAT University, Changa, Anand, Gujarat, 388421, India; Corresponding author: alpeshvala.ec@charusat.ac.in

Received 5 November 2015

ABSTRACT: *This article represented the effective approach to improve the bandwidth and gain response of substrate integrated waveguide antenna (SIW) using novel defected microstrip structure (DMS) technique for Ku band applications. First of all, Horn antenna was designed using SIW technique and it provided gain around 6 dB. Single square loop slots and multiple square loop slots were introduced in SIW based horn antenna and performance analysis have been carried out. Their responses proved that they were not only responding the fundamental mode but also at different high order modes. Creation of multiple square loop slots not only increased bandwidth but also it increased gains more than 8.5 dB. Moreover, the proposed antennas also responding dual frequencies with more than 500 MHz bandwidth, −2 dB side-lobe levels and VSWR was around 1.35. All the structures were simulated using Ansoft high frequency structure simulator. Comparison between results verified the effectiveness of the proposed idea.* © 2016 Wiley Periodicals, Inc. Microwave Opt Technol Lett 58:1577–1582, 2016; View this article online at wileyonlinelibrary.com. DOI 10.1002/mop.29857

Key words: *substrate integrated waveguide; horn antenna; square loop slots; bandwidth; return loss*